JACS
JOURNAL OF THE AMERICAN CHEMICAL SOCIETY
pubs.acs.org/JACS
Article

Observation of Robust Compressed CuO_6 Octahedra and Exotic Spin Structure in $CaCuFe_2O_5$

Maocai Pi, Junye Yang, Jie Zhang, Xubin Ye, Xiao Wang, Lunhua He, Zhiwei Hu, Chien-Te Chen, ChangYang Kuo, Zhao Pan, Yao Shen,* and Youwen Long*

Cite This: J. Am. Chem. Soc. 2025, 147, 4403−4410
Read Online
ACCESS | Metrics & More | Article Recommendations

ABSTRACT: CuO_6 octahedra usually show elongated distortion, leading to active $d_{x^2-y^2}$ orbitals and planar exchange interactions, while compressed CuO_6 octahedra with active $d_{3z^2-r^2}$ orbitals and unidirectional exchange interactions are exceptionally rare. Here, we design and synthesize a new frustrated antiferromagnet $CaCuFe_2O_5$ through a high-pressure and high-temperature approach, in which robust compressed CuO_6 octahedra are realized, separating the Fe_2O_5 sheets that comprise zigzag spin ladders. Magnetic susceptibility and specific heat measurements exhibit a long-range antiferromagnetic order below the Néel temperature of 165 K, which is further confirmed by neutron diffraction. Detailed magnetic refinement reveals a C-type spin structure, with its spin arrangement and orientation distinct from that of the isostructural $CaFe_3O_5$. By constructing a Heisenberg model, we find that this is due to the exchange redistribution between the CuO_6 octahedra and Fe_2O_5 sheets, during which some of the exchange interactions are selectively annihilated due to the specific orientation of the Cu $d_{3z^2-r^2}$ orbitals in the compressed CuO_6 octahedra. Our results provide a unique example of robust compressed CuO_6 octahedra and show that it can selectively annihilate some of the exchange interactions and completely modify the spin structure and magnetic frustration accordingly.

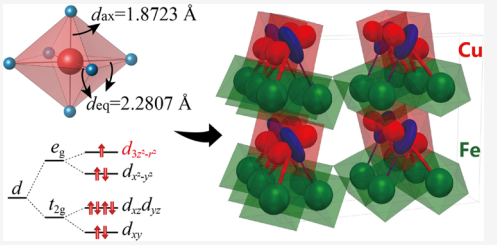

1. INTRODUCTION

Copper-based transition-metal compounds are widely studied in solid-state chemistry and materials sciences.[1] For instance, the past decades have seen extensive exploration of high-temperature superconductivity in $La_{2-x}Ba_xCuO_4$,[2] charge-transfer phenomenon in $LaCu_3Fe_4O_{12}$,[3] and the spin liquid state in $SrCu_2(BO_3)_2$.[4] These fascinating properties are intimately related to the diverse outermost electronic configuration and the wide range of coordinate geometries of copper ions, such as the six-coordinate octahedron, five-coordinate trigonal bipyramid, and four-coordinate square plane, among others.[5] For the six-coordinate octahedral geometry, Cu^{2+}, with a d^9 configuration and a single hole occupying the e_g orbitals, tends to exhibit a lifted orbital degeneracy because of the Jahn−Teller effect combined with intersite Coulomb interactions. More specifically, the single occupancy of $d_{x^2-y^2}$ or $d_{3z^2-r^2}$ orbitals due to the splitting of e_g orbitals takes place simultaneously with the tetragonal elongation or compressed distortion of the octahedron, respectively,[6] leading to appreciable spatial anisotropy.[7] In most cases, the CuO_6 octahedron shows elongated distortion.[8] Hence, the in-plane $d_{x^2-y^2}$ orbitals are pushed toward higher energy and become magnetically active, while the out-of-plane $d_{3z^2-r^2}$ orbitals are fully occupied, being inert, making the z-direction exchange interactions negligible.[9] This is the case for the cuprate superconductors, such as $La_{2-x}Ba_xCuO_4$,[2] where elongated CuO_6 octahedra favor a two-dimensional $d_{x^2-y^2}$ network, which, in fact, largely shapes the magnetism and electronic characters of cuprates and is thought to be intimately related to the unconventional superconductivity.[10−13] In another aspect, active $d_{3z^2-r^2}$ orbitals and inert $d_{x^2-y^2}$ orbitals would be realized in a compressed octahedron, which, however, remains extremely rare and underexplored.

Recently, charge disproportionation has been revealed among the Fe ions in $CaFe_3O_5$, leading to the formula of $CaFe^{2+}Fe_2^{3+}O_5$.[14,15] Within the charge-ordered phase, a long-range collinear magnetic order is developed below ∼280 K with a propagation vector of $\boldsymbol{k} = (1/2, 0, 0)$ and static moment parallel to the c-axis. Notably, the $Fe^{2+}O_6$ octahedra in $CaFe_3O_5$ adopt an appreciable tetrahedral compressed distortion, the influence of which on magnetism, however, is negligible as for Fe^{2+}, with a $3d^6$ configuration in the high-spin state, is only weakly Jahn−Teller active. Nevertheless, a substantial difference is expected if Fe^{2+} can be replaced by other ions with a strong Jahn−Teller response, for example,

Received: October 31, 2024
Revised: January 10, 2025
Accepted: January 10, 2025
Published: January 24, 2025

https://doi.org/10.1021/jacs.4c15326
J. Am. Chem. Soc. 2025, 147, 4403−4410

Cu^{2+}. Thus, the orthorhombic AMM'_2O_5 family (A: alkaline earth metal, M and M': divalent and trivalent cations, respectively) represented by $CaFe_3O_5$ provides an excellent platform for the study of exotic magnetism triggered by compressed octahedra.

Here, through a high-pressure and high-temperature synthesis approach, we managed to completely replace Fe^{2+} with Cu^{2+} in $CaFe_3O_5$, leading to the stabilization of a new frustrated magnet, $CaCuFe_2O_5$. By inspecting its structure with delicate diffraction methods, we find that it comprises exceptional compressed CuO_6 octahedra with active Cu $d_{3z^2-r^2}$ orbitals. Remarkably, the inter-Fe_2O_5-layer exchange interactions bridged by CuO_6 octahedra are redistributed with some almost annihilated. Correspondingly, a long-range C-type antiferromagnetic (AFM) order is realized below 165 K, which presents a distinct moment arrangement and spin orientation from the one in the isostructural $CaFe_3O_5$,[14,15] where no such exchange annihilation takes place.

2. METHODS SECTION

Polycrystalline $CaCuFe_2O_5$ samples were prepared with a high-pressure and high-temperature synthesis method. Highly pure CaO, CuO, and Fe_2O_3 powders were mixed with a 1:1:1 mol ratio and thoroughly ground in an agate mortar within an argon-filled glovebox. Then, the mixture was sealed into a platinum capsule with 3.0 mm in diameter and height and treated at 5 GPa and 1373 K for 30 min in a cubic anvil-type high-pressure apparatus. Afterward, the sample was quenched to room temperature, and the pressure was slowly released. Note that high pressure is necessary here as the synthesis at ambient pressure would lead to poor sample quality and lots of impurities.

Room-temperature synchrotron X-ray powder diffraction (SXRD) pattern was collected using a large Debye−Scherrer camera installed at the BL02B2 beamline (λ = 0.4201 Å) of SPring-8. Neutron powder diffraction (NPD) patterns were collected at the time-of-flight general-purpose powder diffractometer (GPPD) installed at the China Spallation Neutron Source (CSNS).[16] The Rietveld refinements for the SXRD and NPD data were performed using the GSAS[17] and Fullprof[18] programs, respectively. The soft X-ray absorption spectroscopies (XAS) were collected with total electron yield mode at the BL08B beamline of the National Synchrotron Radiation Research Center (NSRRC) in Taiwan. The magnetic susceptibility and magnetization were measured with a SQUID magnetometer (Quantum Design, MPMS 5), and the specific heat data were collected using a physical property measurement system (Quantum Design, PPMS-9T).

3. RESULTS AND DISCUSSION

Figure 1a shows room-temperature SXRD measurements of the $CaCuFe_2O_5$ polycrystalline sample. All of the diffraction peaks can be well fitted with an orthorhombic symmetry $Cmcm$, which is the same as assigned for $CaFe_3O_5$ (i.e., $CaFe^{2+}Fe^{3+}_2O_5$). The refined lattice parameters are a = 3.02866(4) Å, b = 10.10080(1) Å, and c = 12.42223(7) Å. The schematic diagram of the crystal structure of $CaCuFe_2O_5$ is shown in Figure 1b. The edge-shared FeO_6 octahedra form one-dimensional zigzag ladders running along the structural a direction (see Figure 1b,c), which are further connected with each other through corner-shared octahedra along the c-axis. The obtained two-dimensional Fe_2O_5 sheets are stacked along the b direction, separated by a-axis CuO_6 chains constituting edge-shared CuO_6 octahedra. Each CuO_6 octahedron shares all six legend oxygens with adjacent FeO_6 octahedra through an edge-shared connection. The refined structural parameters are presented in Table 1. It is worth noting that the six Cu−O bond lengths in a CuO_6 octahedron are 1.8723 Å × 2 and 2.2807 Å × 4 (see Figure 1d), strongly indicating that the CuO_6 octahedra are substantially compressed.

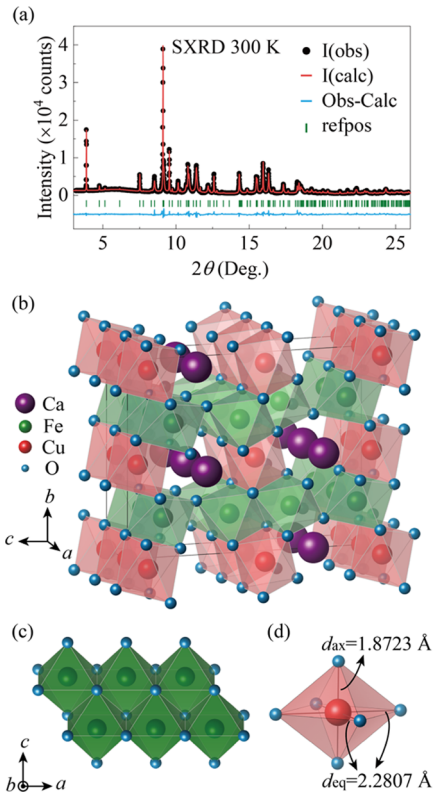

Figure 1. (a) Synchrotron X-ray powder diffraction pattern collected at room temperature and the corresponding structure refinement results. The observed (obs, black dot), calculated (calc, red line), and difference (Obs-Calc, blue line) profiles are shown. The green ticks (refpos) indicate the allowed Bragg reflections. (b) Schematic of the $CaCuFe_2O_5$ crystal structure obtained from the refinement. (c) The local S = 5/2 zigzag spin ladder constituting edge-shared FeO_6 octahedra. (d) The compressed CuO_6 octahedron with a d_{ax} = 1.8723 Å axial and d_{eq} = 2.2807 Å horizontal Cu−O bond length.

We further use temperature-dependent NPD measurements to explore how the lattice structure evolves with temperature. Figure 2a shows the NPD pattern collected at 10 and 300 K, both of which can be well described by the crystal structure determined from the SXRD measurements. Extra magnetic peaks emerge at 10 K and will be discussed subsequently. The refined structure parameters of NPD are presented in Table 1, in which the oxygen locations that can be more precisely determined by NPD are consistent with the SXRD results. No indication of antisite occupation between Cu and Fe can be inferred from the NPD refinement.

Based on these observations, we conclude that robust compressed CuO_6 octahedra are present at both room temperature and low temperature. This phenomenon excludes the dynamic Jahn−Teller effect, which shows different types of distortion at different temperatures. Thus, the compressed CuO_6 octahedra are unique and intrinsic in $CaCuFe_2O_5$ as a result of a synergic effect of the internal electric field generated by all of the ions and can be realized in the absence of the Jahn−Teller effect. It is worth noting that there is a significant symmetry constraint with the $Cmcm$ space group in the $CaFe_3O_5$-type structure, which fixes the x coordinates of all atoms in the lattice of $CaCuFe_2O_5$. The loss of one spatial degree of freedom makes the edge-sharing CuO_6 and FeO_6

https://doi.org/10.1021/jacs.4c15326
J. Am. Chem. Soc. 2025, 147, 4403−4410

Table 1. Refined Crystal Parameters of $CaCuFe_2O_5$ Based on SXRD and NPD Diffraction Patterns[a]

parameter	300 K SXRD	300 K NPD	10 K NPD
a (Å)	3.02866(4)	3.02747(4)	3.01805(3)
b (Å)	10.10080(1)	10.08856(1)	10.07330(7)
c (Å)	12.42223(7)	12.38791(2)	12.36720(1)
Ca_y	0.52939(4)	0.52798(9)	0.52404(3)
Ca_z	0.25	0.25	0.25
Fe_y	0.27460(5)	0.27412(3)	0.27512(5)
Fe_z	0.10909(1)	0.10831(1)	0.10784(7)
$O1_y$	0.20687(3)	0.20097(5)	0.20310(2)
$O1_z$	0.25	0.25	0.25
$O2_y$	0.65521(8)	0.65173(8)	0.64800(4)
$O2_z$	0.44597(6)	0.44771(1)	0.44861(4)
$O3_y$	0.90995(2)	0.90981(4)	0.91185(6)
$O3_z$	0.13174(5)	0.13388(9)	0.13656(4)
Fe−O1 (×1) (Å)	1.87936(2)	1.90407(3)	1.90192(3)
Fe−O2 (×2) (Å)	2.05311(4)	2.07306(2)	2.09863(6)
Fe−O2 (×1) (Å)	2.14676(1)	2.12549(4)	2.11604(3)
Fe−O3 (×2) (Å)	2.05947(7)	2.06535(2)	2.07372(7)
Cu−O2 (×2) (Å)	1.87229(6)	1.89169(3)	1.90807(4)
Cu−O3 (×4) (Å)	2.28068(2)	2.24814(3)	2.21443(2)
∠Fe−O1−Fe (deg)	137.30(5)	134.39(1)	135.15(3)
∠Fe−O2−Fe (deg)	96.91 (1)	95.95(1)	94.94(9)
∠Fe−O2−Fe (deg)	95.05(9)	93.80(3)	91.95(2)
∠Fe−O3−Fe (deg)	94.66(4)	94.26(5)	93.38(6)
∠Fe−O2−Cu (deg)	90.69(1)	90.59(6)	90.93(2)
∠Fe−O2−Cu (deg)	87.09(0)	88.08(5)	88.81(4)
∠Cu−O2−Cu (deg)	83.20(8)	84.65(1)	85.91(4)
Rwp (%)	3.24	7.02	8.75
Rp (%)	2.13	9.19	11.1

[a]Cu^{2+} is located at the origin, and the x-axis coordinates of all atoms are fixed at zero under the symmetry constraint of the $Cmcm$ space group.

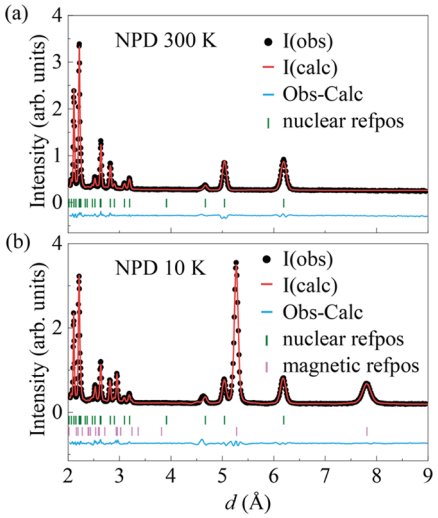

Figure 2. Neutron powder diffraction patterns along with the refinement results at (a) 300 and (b) 10 K. The observed (black dot), calculated (red line), and difference (blue line) profiles are shown. The green and pink ticks indicate the nuclear and magnetic peaks, respectively.

octahedra network rather stiff and the compressed CuO_6 octahedra robust. In fact, the AMM'_2O_5 family is related to a collapsed version of the spinel structure, termed postspinel. The chemical formula can be expressed as $(AM'_2O_4)(MO)_n$ where n stands for the number of (MO) slabs that are alternately stacked with (AM'_2O_4) blocks. For instance, $CaFe_4O_6$ and $CaFe_5O_7$ materials correspond to the n = 2 and 3 members,[19] and $CaCuFe_2O_5$ can also be written as $(CaFe_2O_4)(CuO)$. As a collapsed version, the postspinel structure is "crowded" and has a much higher density than the cubic spinel. As an example, $CdFe_2O_4$ crystallizes into the orthorhombic $CaFe_2O_4$-type structure with the space group $Pnma$ at high pressure and is significantly denser than the ambient cubic phase by 11.5%.[20] In such a case, compressed octahedra are favorable, which is one of the origins of robust compressed CuO_6 octahedra in $CaCuFe_2O_5$.

Based on the refined Cu−O and Fe−O bond lengths, we can calculate the bond valence sum (BVS) of Cu and Fe, which gives +1.97 and +2.91, respectively, suggesting the Cu^{2+} and Fe^{3+} valence states. To further confirm this result, we performed XAS measurements at the Cu and Fe-L edges, which are highly sensitive to the valence state of 3d elements,[21] as well as the local environment.[22,23] Figure 3 shows the XAS

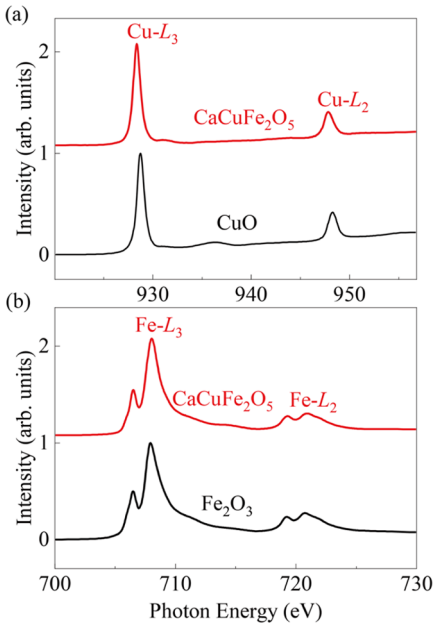

Figure 3. XAS measurements of $CaCuFe_2O_5$ at (a) Cu-$L_{2,3}$ edges and (b) Fe-$L_{2,3}$ edges. The XAS data for CuO and Fe_2O_3 are also presented for reference.

spectra at the Fe-$L_{2,3}$ and Cu-$L_{2,3}$ edges of $CaCuFe_2O_5$ together with CuO as a Cu^{2+} reference and Fe_2O_3 as a high-spin Fe^{3+} reference. The excellent consistency between the title compound and reference materials indicates that a valence configuration of $CaCu^{2+}Fe_2^{3+}O_5$ is realized, with the Fe^{3+} ($3d^5$) ions being in the high-spin state (S = 5/2) in an octahedral coordination. Correspondingly, its magnetism is mostly isotropic, but weak anisotropy is expected due to the slight distortion of the FeO_6 octahedra. In sharp contrast, for the Cu^{2+} ion with a $3d^9$ configuration in a significantly compressed CuO_6 octahedron, the active $d_{3z^2-r^2}$ orbitals and inert $d_{x^2-y^2}$ orbitals would lead to substantial spatial anisotropy and redistribution of the exchange interactions, which would strongly modify the magnetism of $CaCuFe_2O_5$.

To explore the magnetic properties of $CaCuFe_2O_5$, we made a detailed investigation into its thermodynamic behaviors.

https://doi.org/10.1021/jacs.4c15326
J. Am. Chem. Soc. 2025, 147, 4403−4410

Figure 4a depicts the temperature dependence of the magnetic susceptibility χ, in which a peak-like anomaly is presented at

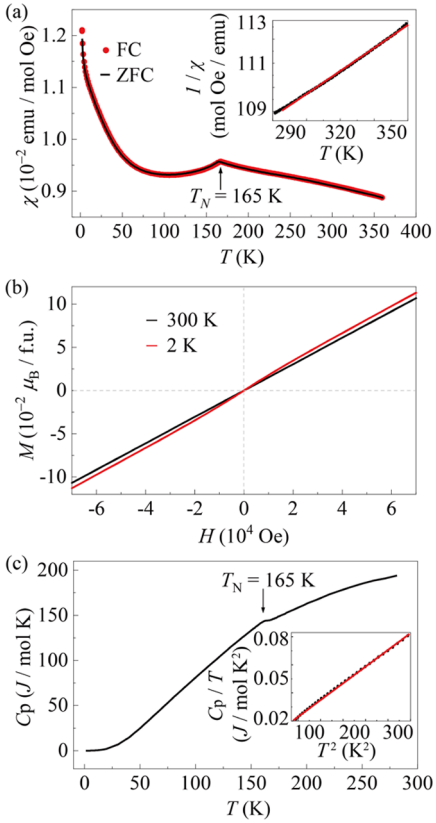

Figure 4. (a) Temperature dependence of the magnetic susceptibility measured at 1000 Oe with ZFC and FC modes. The inset shows the inverse susceptibility with CW fitting between 290 and 360 K. (b) The field-dependent magnetization measured at 2 and 300 K. f.u., formula units. (c) Temperature dependence of the specific heat down to 2 K in zero field. The inset shows the fitting results with $Cp/T = \beta T^2$.

$T_N \approx 165$ K, suggesting the occurrence of a long-range AFM transition. No splitting is observed between the zero-field-cooling (ZFC) and field-cooling (FC) curves. The inverse susceptibility shows the Curie–Weiss (CW) behavior above 280 K, leading to a fitted CW temperature of $\theta_{CW} = -2005$ K. Correspondingly, a frustration factor $f = |\theta_{CW}|/T_N \approx 12.15$ is obtained, highlighting the intrinsic magnetic frustration.[24] A linear behavior with no hint of saturation is observed in the magnetic field dependence of the magnetization, consistent with the AFM ground state (Figure 4b). The magnetic transition is also available in the specific heat measurements in which a λ-type anomaly takes place around T_N (see Figure 4c). The low-temperature specific heat can be effectively described by $Cp/T = \beta T^2$, where $\beta = 2.84 \times 10^{-4}$ J/mol·K^4, indicating the phonon and the AFM contributions. Note that the current $CaCuFe_2O_5$ is electrical insulating as the resistivity exceeds 1×10^7 Ωcm at room temperature. Hence, no electronic contribution is expected to occur in the specific heat data.

After establishing the emergence of magnetic order below $T_N \approx 165$ K in $CaCuFe_2O_5$, we now return to the NPD data to determine its spin structure. At 10 K, extra peaks with comparable peak width emerge in the NPD pattern (Figure 2b), indicating the appearance of a long-range static magnetic order. Magnetic refinement confirms that all of the magnetic reflections at low temperature can be interpreted by a single propagation vector, $\boldsymbol{k} = (1, 0, 0)$. The detailed spin structure obtained from the refinement is presented in Figure 5a, in which all of the spin moments, including the ones for Cu^{2+} and Fe^{3+}, are antiferromagnetically aligned along the b and c directions while ferromagnetically aligned along the a direction. This is in sharp contrast to the isostructural $CaFe_3O_5$ where along the a direction, both the Fe^{2+} and Fe^{3+} moments are arranged in an antiparallel manner, with a propagation vector of $\boldsymbol{k} = (1/2, 0, 0)$.[14,15] The spin moments are oriented along the a direction in $CaCuFe_2O_5$ instead of the c direction in $CaFe_3O_5$, which might be caused by the slight change of the weak anisotropy due to the delicate octahedral distortion. The refined ordered spin moment is 0.9 μ_B for Cu^{2+}, close to the theoretical value, while 3.2 μ_B for Fe^{3+}, much smaller than the theoretical expectation, which is ascribed to the magnetic frustration.[25,26]

To interpret the observed exotic spin structure of $CaCuFe_2O_5$ and its distinction from $CaFe_3O_5$, we adopt the localized Heisenberg model

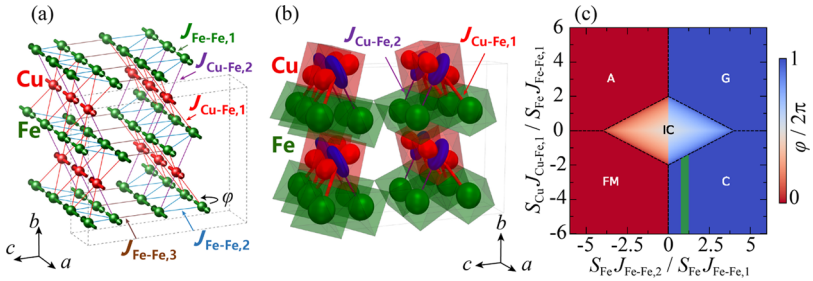

Figure 5. Modeling of the spin structure of $CaCuFe_2O_5$. (a) C-type spin structure of $CaCuFe_2O_5$ obtained from the NPD refinement. Five inequivalent nearest neighbor exchange interaction paths are annotated with different colors. Note that only the $J_{Fe-Fe,3}$ bonds constitute corner-shared octahedra (bond angle around 137.3°), while the others are bridged through edge-shared octahedra. (b) Schematic of the active electronic orbitals of Fe^{3+} and Cu^{2+} in $CaCuFe_2O_5$. For Fe^{3+} ($3d^5$) with a high-spin state ($S = 5/2$), an isotropic sphere is expected, while for Cu ($3d^9$) with compressed CuO_6 octahedra, only $d_{3z^2-r^2}$ orbitals contribute to the magnetism. Due to the unique orientation of the $d_{3z^2-r^2}$ orbitals, $J_{Cu-Fe,2}$ is expected to be significantly suppressed. (c) The calculated magnetic phase diagram of the spin Hamiltonian proposed for $CaCuFe_2O_5$. Five distinct phases are presented, including the A-type (A), G-type (G), C-type (C), ferromagnetic (FM), and incommensurate (IC) states. The green vertical bar indicates the parameter space expected for $CaCuFe_2O_5$. Note that $J_{Fe-Fe,3}$ is irrelevant here since it is not frustrated. φ denotes the phase difference between the adjacent spins within a ladder leg as marked in panel (a). S_{Fe} and S_{Cu} spin sizes for Fe^{3+} and Cu^{2+}, respectively.

https://doi.org/10.1021/jacs.4c15326
J. Am. Chem. Soc. 2025, 147, 4403–4410

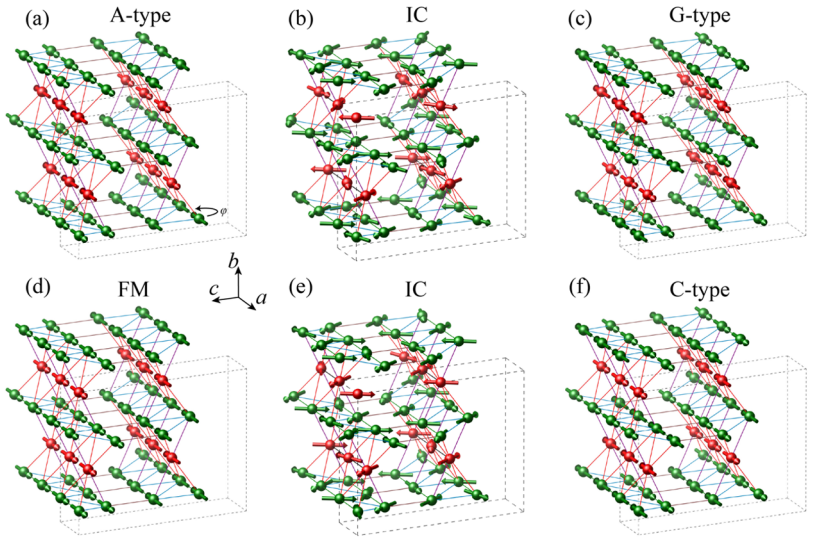

Figure 6. Schematic of the spin structures presented in the phase diagram. Five distinct phases are presented, including the A-type (A), G-type (G), C-type (C), ferromagnetic (FM), and incommensurate states (IC). Two representative IC spin structure are shown in panels (b) and (e). The notations used here are borrowed from the magnetic structure labels used for cubic systems to distinguish the various phases in the phase diagram, representing the different intra-Fe_2O_5-ladder and inter−Fe-Cu spin arrangements.

$$H = \sum_{\langle ij \rangle} J_{ij} S_i \cdot S_j \tag{1}$$

where J_{ij} denotes the nearest neighbor (NN) exchange interactions and $\langle ij \rangle$ represents the corresponding bonds.

By inspecting the lattice structure, we find that there are five inequivalent NN exchange interactions, $J_{Fe-Fe,1}$, $J_{Fe-Fe,2}$, $J_{Fe-Fe,3}$, $J_{Cu-Fe,1}$, and $J_{Cu-Fe,2}$, as shown in Figure 5a. Among all of these interactions, $J_{Fe-Fe,3}$ is not frustrated by symmetry, while a profound competition is expected for the rest of them. This scenario applies for $CaFe_3O_5$.[15] For $CaCuFe_2O_5$, however, the situation is quite different. With a $3d^9$ configuration of Cu^{2+} in a compressed octahedron, a single hole occupies the $d_{3z^2-r^2}$ orbital, making it the only one that is magnetically active. Since the $d_{3z^2-r^2}$ orbital is highly unidirectional, pointing toward one of the Fe^{3+} spin ladder legs (see Figure 5b), $J_{Cu-Fe,1}$ is enhanced due to the large orbital overlapping. For the same reason, $J_{Cu-Fe,2}$ is significantly suppressed and can be neglected in the Hamiltonian. Consequently, there are three free parameters left: $J_{Fe-Fe,1}$, $J_{Fe-Fe,2}$, and $J_{Cu-Fe,1}$. To obtain the phase diagram, we treat $S_{Fe}J_{Fe-Fe,2}/S_{Fe}J_{Fe-Fe,1}$ and $S_{Cu}J_{Cu-Fe,1}/S_{Fe}J_{Fe-Fe,1}$ as variants. Note that we keep S_{Fe} and S_{Cu} here due to the distinct spin size for high-spin Fe^{3+} and Cu^{2+}. The Hamiltonian is solved through the linear spin wave theory using SPINW software,[27] and the phase diagram is presented in Figure 5c. Here, we assume an easy *a*-axis when the spin structure is linear and an easy *ac* plane when it is nonlinear. Assuming $J_{Fe-Fe,1}$ being AFM, a stronger ferromagnetic (FM) $J_{Fe-Fe,2}$ would overwhelm $J_{Fe-Fe,1}$, resulting in FM Fe_2O_5 zigzag spin ladders. The Cu^{2+} chains are also FM, and their alignment with the Fe_2O_5 ladders depends on the $J_{Cu-Fe,1}$. If $J_{Cu-Fe,1}$ is AFM, then an A-type spin structure is realized (see Figure 6a). If it is FM, then an FM structure is stabilized instead (see Figure 6d). Note that the inter-Fe_2O_5-ladder interactions $J_{Fe-Fe,3}$ are always AFM due to the 137.3° ∠Fe−O1−Fe. When $J_{Fe-Fe,2}$ is strongly AFM and also overwhelms $J_{Fe-Fe,1}$, the Fe_2O_5 zigzag ladders exhibit FM intraleg and AFM interleg spin alignments. Again, the Cu^{2+} chains are FM, and AFM $J_{Cu-Fe,1}$ leads to a G-type spin structure (see Figure 6c), while FM $J_{Cu-Fe,1}$ leads to a C-type one (see Figure 6f). It should be noted that whether $J_{Cu-Fe,1}$ is FM or AFM, it will effectively provide FM couplings to one of the legs of the Fe_2O_5 ladder and competes with AFM $J_{Fe-Fe,1}$. Thus, even when $J_{Fe-Fe,2}$ is small, a G-type or C-type spin structure can be realized. The frustration is maximized when $J_{Fe-Fe,1}$, dressed with $J_{Cu-Fe,1}$, is comparable to $J_{Fe-Fe,2}$. In that case, incommensurate nonlinear spin structures with a propagation of $(\varphi/2\pi, 0, 0)$ are realized (see Figure 6b,e).

Among all five possible spin configurations discussed above, the C-type state is consistent with the spin structure of $CaCuFe_2O_5$. This can be qualitatively accounted for considering that $J_{Fe-Fe,1}$ and $J_{Fe-Fe,2}$ should be comparable due to the similar bond lengths (3.0287 Å for $J_{Fe-Fe,1}$ and 3.1442 Å for $J_{Fe-Fe,2}$) and bond angles (∠Fe−O3−Fe = 94.6° for $J_{Fe-Fe,1}$ and ∠Fe−O2−Fe = 95.0° for $J_{Fe-Fe,2}$), and the fact that they are both bridged by edge-sharing FeO_6 octahedra. In another aspect, the exchange interaction between the Cu $d_{3z^2-r^2}$ orbital and Fe orbitals with a half-filled 3*d* shell is complex. According to the Goodenough−Kanamori−Anderson rules,[28] for the edge-sharing case with a close-to-90° bond angle, the superexchange interaction between $d_{3z^2-r^2}$ and d_{xz} is strongly AFM, while those between $d_{3z^2-r^2}$ and the rest of the 3*d* orbitals are weakly ferromagnetic (FM), the combination of which can be either AFM or FM. Based on the results for $CaCuFe_2O_5$, an FM $J_{Cu-Fe,1}$ is realized eventually, and the corresponding parameter space is indicated by the green shadow in Figure 5c. The presence of $J_{Cu-Fe,1}$ but the annihilation of $J_{Cu-Fe,2}$ has multiple consequences, one of which is the suppression of geometric frustration. Inspecting the Fe^{3+} zigzag spin ladder without considering the interplane interactions ($J_{Cu-Fe,1}$ and $J_{Cu-Fe,2}$), there is strong competition between the intra- and interleg interactions ($J_{Fe-Fe,1}$ and $J_{Fe-Fe,2}$, respectively), resulting in incommensurate spin arrangements as indicated in the phase diagram with zero $J_{Cu-Fe,1}$ (see Figure 5c). In fact, the Fe_2O_5 sheets resemble the distorted triangular lattice, which also shows a noncollinear spin structure due to geometric frustration.[29] Nonzero $J_{Cu-Fe,1}$ introduces an effective FM term for the intraleg interactions, competing

https://doi.org/10.1021/jacs.4c15326
J. Am. Chem. Soc. 2025, 147, 4403−4410

with $J_{Fe-Fe,1}$, hence tipping the balance. When $J_{Cu-Fe,1}$ is strong enough, the interleg AFM interactions will overwhelm the intraleg ones, leading to FM ladder legs, as is the case for $CaCuFe_2O_5$.

The obtained spin structure for $CaCuFe_2O_5$ is a direct result of the annihilation of $J_{Cu-Fe,2}$ induced by compressed CuO_6 octahedra. It should be noted that such a spin configuration cannot be stabilized if $J_{Cu-Fe,2}$ is also present. Other than $CaCuFe_2O_5$ reported here, there are only a few examples that are shown to contain compressed CuO_6 octahedra. For instance, $Ba_2CuO_{4-\delta}$ is a newly found cuprate superconductor proposed to present compressed CuO_6 octahedra with a superconducting transition temperature as high as 70 K.[30] However, it is also discovered that the diffraction data can be partially accounted for by considering elongated octahedra with oxygen vacancies.[31] Thus, its real structure remains controversial. In another aspect, unambiguous evidence for compressed CuO_6 octahedra has been found in the spin chain system $Cu_3Mo_2O_9$, in which only one-third of the Cu ions reside in the compressed octahedra, whereas others are coordinated in a pyramidal environment, leading to appreciable complexity of the magnetism.[32,33] The Kagomé lattice volborthite $Cu_3V_2O_7(OH)_2{\cdot}2H_2O$ is another candidate, and compressed CuO_6 octahedra are found at high temperature,[34,35] while at low temperature, before the magnetic order kicks in, there is a subtle structural transition during which the compressed CuO_6 octahedra are stretched and become elongated eventually, leading to an orbital switching.[34,36] Hence, the magnetism in this material is also established on elongated CuO_6 octahedra instead of compressed ones.

In addition to copper oxides, compressed CuX_6 octahedra were also observed in some halide perovskites, such as K_2CuF_4, which is isostructural to the cuprate superconductor La_2CuO_4. However, an antiferrodistortive arrangement of elongated octahedral is also proposed for this material.[37] Meanwhile, well-defined compressed CuF_6 octahedra were observed in $KAlCuF_6$,[38,39] which is stabilized by heavily tilted corner-shared CuF_6 octahedra with a Cu−F−Cu bond angle of 125.9° that is very close to the edge-shared case. β-$CuX_2(NH_3)_2$ (X = Cl or Br) is another member but with an edge-shared $[Cu(X)_4(NH_3)_2]$ complex.[40] Overall, the material reported in the current work, $CaCuFe_2O_5$, is a rare example composed of pure compressed CuO_6 octahedra and realizes a novel spin structure that can be stabilized only with selectively annihilated exchange interactions due to the unidirectional Cu $d_{3z^2-r^2}$ orbital orientations.

4. CONCLUSIONS

In summary, we have successfully prepared a new frustrated antiferromagnet $CaCuFe_2O_5$ at high-pressure and high-temperature conditions. The Rietveld analysis based on the powder SXRD and NPD patterns reveals robust compressed CuO_6 octahedra, which originate mainly from the cooperative effect of the internal electric field and lead to dominant $d_{3z^2-r^2}$ orbital contributions to the magnetism. The specific orientation of the $d_{3z^2-r^2}$ orbital selectively annihilates some of the exchange interactions between the Cu and Fe ions. Consequently, the magnetic frustration is partially released, and a novel spin structure distinct from that of the isostructural $CaFe_3O_5$ is stabilized. Our results provide a one-of-a-kind scenario with compressed CuO_6 octahedra and show that by modifying the delicate structural distortion, we can selectively annihilate some of the exchange interactions and change the magnetism in a controlled manner.

AUTHOR INFORMATION

Corresponding Authors

Yao Shen − *Beijing National Laboratory for Condensed Matter Physics, Institute of Physics, Chinese Academy of Sciences, Beijing 100190, China; School of Physical Sciences, University of Chinese Academy of Sciences, Beijing 100049, China*; Email: yshen@iphy.ac.cn

Youwen Long − *Beijing National Laboratory for Condensed Matter Physics, Institute of Physics, Chinese Academy of Sciences, Beijing 100190, China; School of Physical Sciences, University of Chinese Academy of Sciences, Beijing 100049, China; Songshan Lake Materials Laboratory, Dongguan, Guangdong 523808, China*; orcid.org/0000-0002-8587-7818; Email: ywlong@iphy.ac.cn

Authors

Maocai Pi − *Beijing National Laboratory for Condensed Matter Physics, Institute of Physics, Chinese Academy of Sciences, Beijing 100190, China; School of Physical Sciences, University of Chinese Academy of Sciences, Beijing 100049, China*

Junye Yang − *Institute of High Energy Physics, Chinese Academy of Sciences, Beijing 100049, China; Spallation Neutron Source Science Center, Dongguan 523803, China*

Jie Zhang − *Beijing National Laboratory for Condensed Matter Physics, Institute of Physics, Chinese Academy of Sciences, Beijing 100190, China; School of Physical Sciences, University of Chinese Academy of Sciences, Beijing 100049, China*; orcid.org/0009-0006-9055-2969

Xubin Ye − *Beijing National Laboratory for Condensed Matter Physics, Institute of Physics, Chinese Academy of Sciences, Beijing 100190, China*; orcid.org/0000-0002-5739-8318

Xiao Wang − *Beijing National Laboratory for Condensed Matter Physics, Institute of Physics, Chinese Academy of Sciences, Beijing 100190, China*; orcid.org/0000-0001-8139-4192

Lunhua He − *Beijing National Laboratory for Condensed Matter Physics, Institute of Physics, Chinese Academy of Sciences, Beijing 100190, China; Spallation Neutron Source Science Center, Dongguan 523803, China*

Zhiwei Hu − *Max Planck Institute for Chemical Physics of Solids, Dresden 01187, Germany*; orcid.org/0000-0003-0324-2227

Chien-Te Chen − *National Synchrotron Radiation Research Center, Hsinchu 300092, Taiwan*

ChangYang Kuo − *National Synchrotron Radiation Research Center, Hsinchu 300092, Taiwan; Department of Electrophysics, National Yang Ming Chiao Tung University, Hsinchu 30010, Taiwan*

Zhao Pan − *Beijing National Laboratory for Condensed Matter Physics, Institute of Physics, Chinese Academy of Sciences, Beijing 100190, China; School of Physical Sciences, University of Chinese Academy of Sciences, Beijing 100049, China*; orcid.org/0000-0002-8693-2508

Complete contact information is available at: https://pubs.acs.org/10.1021/jacs.4c15326

Notes

The authors declare no competing financial interest.

https://doi.org/10.1021/jacs.4c15326
J. Am. Chem. Soc. 2025, 147, 4403−4410

■ ACKNOWLEDGMENTS

This work was supported by the National Key R&D Program of China (Grant No. 2021YFA1400300), the National Natural Science Foundation of China (Grant Nos. 12425403, 12261131499, 12304268, 12304159, 11934017, 11921004), the China Postdoctoral Science Foundation (Grant No. 2023M743741), and the Chinese Academy of Sciences (Grant No. XDB33000000). The neutron diffraction experiments were supported by the Open Fund of the China Spallation Neutron Source Songshan Lake Science City (Grant No. KFKT2023A08). The synchrotron X-ray powder diffraction experiments were performed at SPring-8 with the approval of the Japan Synchrotron Radiation Research Institute (2024A1506 and 2024A1695). The authors acknowledge support from the Max Planck-POSTECH-Hsinchu Center for Complex Phase Materials.

■ REFERENCES

(1) Belsky, A.; Hellenbrandt, M.; Karen, V. L.; Luksch, P. New developments in the Inorganic Crystal Structure Database (ICSD): accessibility in support of materials research and design. *Acta Crystallogr., Sect. B:Struct. Sci.* **2002**, *58* (3), 364−369.

(2) Bednorz, J. G.; Müller, K. A. Possible high T_c superconductivity in the Ba−La−Cu−O system. *Z. Phys. B:Condens. Matter* **1986**, *64* (2), 189−193.

(3) Long, Y. W.; Hayashi, N.; Saito, T.; Azuma, M.; Muranaka, S.; Shimakawa, Y. Temperature-induced A−B intersite charge transfer in an A-site-ordered $LaCu_3Fe_4O_{12}$ perovskite. *Nature* **2009**, *458* (7234), 60−63.

(4) Smith, R. W.; Keszler, D. A. Synthesis, structure, and properties of the orthoborate $SrCu_2(BO_3)_2$. *J. Solid State Chem.* **1991**, *93* (2), 430−435.

(5) Halcrow, M. A. Jahn−Teller distortions in transition metal compounds, and their importance in functional molecular and inorganic materials. *Chem. Soc. Rev.* **2013**, *42* (4), 1784−1795.

(6) Griffith, J. S.; Orgel, L. Ligand-field theory. *Q. Rev., Chem. Soc.* **1957**, *11* (4), 381−393.

(7) Kugel, K. I.; Khomskĭ, D. The Jahn-Teller effect and magnetism: transition metal compounds. *Sov. Phys. Usp.* **1982**, *25* (4), No. 231.

(8) Eby, R. K.; Hawthorne, F. Structural relations in copper oxysalt minerals. I. Structural hierarchy. *Acta Crystallogr., Sect. B:Struct. Sci.* **1993**, *49* (1), 28−56.

(9) Sala, M. M.; Bisogni, V.; Aruta, C.; Balestrino, G.; Berger, H.; Brookes, N.; De Luca, G.; Di Castro, D.; Grioni, M.; Guarise, M.; et al. Energy and symmetry of dd excitations in undoped layered cuprates measured by Cu L_3 resonant inelastic x-ray scattering. *New J. Phys.* **2011**, *13* (4), No. 043026.

(10) Kastner, M. A.; Birgeneau, R.; Shirane, G.; Endoh, Y. Magnetic, transport, and optical properties of monolayer copper oxides. *Rev. Mod. Phys.* **1998**, *70* (3), 897.

(11) Tranquada, J. M.; Dean, M. P.; Li, Q. Superconductivity from charge order in cuprates. *J. Phys. Soc. Jpn.* **2021**, *90* (11), No. 111002.

(12) Keimer, B.; Kivelson, S. A.; Norman, M. R.; Uchida, S.; Zaanen, J. From quantum matter to high-temperature superconductivity in copper oxides. *Nature* **2015**, *518* (7538), 179−186.

(13) Lee, P. A.; Nagaosa, N.; Wen, X.-G. Doping a Mott insulator: Physics of high-temperature superconductivity. *Rev. Mod. Phys.* **2006**, *78* (1), 17−85.

(14) Hong, K. H.; Arevalo-Lopez, A. M.; Cumby, J.; Ritter, C.; Attfield, J. P. Long range electronic phase separation in $CaFe_3O_5$. *Nat. Commun.* **2018**, *9* (1), No. 2975.

(15) Cassidy, S. J.; Orlandi, F.; Manuel, P.; Clarke, S. J. Single phase charge ordered stoichiometric $CaFe_3O_5$ with commensurate and incommensurate trimeron ordering. *Nat. Commun.* **2019**, *10* (1), No. 5475.

(16) He, L.; Deng, S.; Shen, F.; Chen, J.; Lu, H.; Tan, Z.; Zheng, H.; Hao, J.; Zhao, D.; Ma, Q. The performance of general purpose powder diffractometer at CSNS. *Nucl. Instrum. Methods Phys. Res., Sect. A* **2023**, *1054*, No. 168414.

(17) Toby, B. H.; Von Dreele, R. B. GSAS-II: the genesis of a modern open-source all purpose crystallography software package. *J. Appl. Crystallogr.* **2013**, *46* (2), 544−549.

(18) Rodríguez-Carvajal, J. Recent advances in magnetic structure determination by neutron powder diffraction. *Phys. B* **1993**, *192* (1−2), 55−69.

(19) Evrard, O.; Malaman, B.; Jeannot, F.; Courtois, A.; Alebouyeh, H.; Gerardin, R. Mise en évidence de $CaFe_4O_6$ et détermination des structures cristallines des ferrites de calcium $CaFe_{2+n}O_{4+n}$ (n= 1, 2, 3): nouvel exemple d'intercroissance. *J. Solid State Chem.* **1980**, *35* (1), 112−119.

(20) Li, B.; Ye, X.; Wang, X.; Zhang, J.; Lu, D.; Zhao, H.; Pi, M.; Hu, Z.; Lin, H.-J.; Chen, C.-T.; et al. High-Pressure-Stabilized Post-Spinel Phase of $CdFe_2O_4$ with Distinct Magnetism from Its Ambient-Pressure Spinel Phase. *Inorg. Chem.* **2023**, *62* (23), 9139−9145.

(21) Deng, H.; Liu, M.; Dai, J.; Hu, Z.; Kuo, C.; Yin, Y.; Yang, J.; Wang, X.; Zhao, Q.; Xu, Y.; et al. Strong enhancement of spin ordering by A-site magnetic ions in the ferrimagnet $CaCu_3Fe_2Os_2O_{12}$. *Phys. Rev. B* **2016**, *94* (2), No. 024414.

(22) Burnus, T.; Hu, Z.; Wu, H.; Cezar, J.; Niitaka, S.; Takagi, H.; Chang, C. F.; Brookes, N. B.; Lin, H.-J.; Jang, L.; et al. X-ray absorption and x-ray magnetic dichroism study on Ca_3CoRhO_6 and Ca_3FeRhO_6. *Phys. Rev. B* **2008**, *77* (20), No. 205111.

(23) Hollmann, N.; Valldor, M.; Wu, H.; Hu, Z.; Qureshi, N.; Willers, T.; Chin, Y.-Y.; Cezar, J.; Tanaka, A.; Brookes, N.; Tjeng, L. H. Orbital occupation and magnetism of tetrahedrally coordinated iron in $CaBaFe_4O_7$. *Phys. Rev. B* **2011**, *83* (18), No. 180405.

(24) Balents, L. Spin liquids in frustrated magnets. *Nature* **2010**, *464* (7286), 199−208.

(25) Petit, S.; Lhotel, E.; Canals, B.; Ciomaga Hatnean, M.; Ollivier, J.; Mutka, H.; Ressouche, E.; Wildes, A. R.; Lees, M. R.; Balakrishnan, G. Observation of magnetic fragmentation in spin ice. *Nat. Phys.* **2016**, *12* (8), 746−750.

(26) Banerjee, A.; Bridges, C.; Yan, J.-Q.; Aczel, A.; Li, L.; Stone, M.; Granroth, G.; Lumsden, M.; Yiu, Y.; Knolle, J.; et al. Proximate Kitaev quantum spin liquid behaviour in a honeycomb magnet. *Nat. Mater.* **2016**, *15* (7), 733−740.

(27) Toth, S.; Lake, B. Linear spin wave theory for single-Q incommensurate magnetic structures. *J. Phys.: Condens. Matter* **2015**, *27* (16), No. 166002.

(28) Goodenough, J. *Magnetism and the Chemical Bond*; Interscience, 1963.

(29) Toth, S.; Lake, B.; Hradil, K.; Guidi, T.; Rule, K.; Stone, M.; Islam, A. Magnetic soft modes in the distorted triangular antiferromagnet α-$CaCr_2O_4$. *Phys. Rev. Lett.* **2012**, *109* (12), No. 127203.

(30) Li, W. M.; Zhao, J.; Cao, L.; Hu, Z.; Huang, Q.; Wang, X.; Liu, Y.; Zhao, G.; Zhang, J.; Liu, Q.; et al. Superconductivity in a unique type of copper oxide. *Proc. Natl. Acad. Sci. U.S.A.* **2019**, *116* (25), 12156−12160.

(31) Fumagalli, R.; Nag, A.; Agrestini, S.; Garcia-Fernandez, M.; Walters, A. C.; Betto, D.; Brookes, N. B.; Braicovich, L.; Zhou, K.-J.; Ghiringhelli, G.; Moretti Sala, M. Crystalline and magnetic structure of $Ba_2CuO_{3+\delta}$ investigated by x-ray absorption spectroscopy and resonant inelastic x-ray scattering. *Phys. C* **2021**, *581*, No. 1353810.

(32) Vilminot, S.; André, G.; Kurmoo, M. Magnetic properties and magnetic structure of $Cu_3Mo_2O_9$. *Inorg. Chem.* **2009**, *48* (6), 2687−2692.

(33) Hosaka, T.; Hachiuma, S.; Kuroe, H.; Sekine, T.; Hase, M.; Oka, K.; Ito, T.; Eisaki, H.; Fujisawa, M.; Okubo, S. Magnetic and electric properties in the distorted tetrahedral spin chain system $Cu_3Mo_2O_9$. In *Journal of Physics: Conference Series*; IOP Publishing, 2012; Vol. *400*, p 032022.

(34) Yoshida, H.; Yamaura, J.-i.; Isobe, M.; Okamoto, Y.; Nilsen, G. J.; Hiroi, Z. Orbital switching in a frustrated magnet. *Nat. Commun.* **2012**, *3* (1), No. 860.

https://doi.org/10.1021/jacs.4c15326
J. Am. Chem. Soc. 2025, 147, 4403−4410

(35) Hiroi, Z.; Ishikawa, H.; Yoshida, H.; Yamaura, J.-i.; Okamoto, Y. Orbital transitions and frustrated magnetism in the kagome-type copper mineral volborthite. *Inorg. Chem.* **2019**, *58* (18), 11949−11960.
(36) Janson, O.; Furukawa, S.; Momoi, T.; Sindzingre, P.; Richter, J.; Held, K. Magnetic behavior of volborthite $Cu_3V_2O_7(OH)_2{\cdot}2H_2O$ determined by coupled trimers rather than frustrated chains. *Phys. Rev. Lett.* **2016**, *117* (3), No. 037206.
(37) Khomskii, D.; Kugel, K. Orbital and magnetic structure of two-dimensional ferromagnets with Jahn-Teller ions. *Solid State Commun.* **1973**, *13* (7), 763−766.
(38) Wingefeld, G.; Hoppe, R. Über $KCuAlF_6$. *Z. Anorg. Allg. Chem.* **1984**, *516* (9), 223−228.
(39) Finnie, K.; Dubicki, L.; Krausz, E. R.; Riley, M. J. Spectroscopic verification of a tetragonal compression in an octahedral copper (II) compound. *Inorg. Chem.* **1990**, *29* (19), 3908−3910.
(40) Hanic, F.; Čakajdová, J. Die Kristallstruktur von $Cu(NH_3)_2Br_2$ und $Cu(NH_3)_2Cl_2$. *Acta Crystallogr.* **1958**, *11* (9), 610−612.

https://doi.org/10.1021/jacs.4c15326
J. Am. Chem. Soc. 2025, 147, 4403−4410